ORIGINAL ARTICLE

High photocatalytic capacity of porous ceramic-based powder doped with MgO

Dikra Bouras[1] · Mamoun Fellah[2] · Abla Mecif[1] · Régis Barillé[3] · Aleksei Obrosov[4] · Mohammed Rasheed[5]

Abstract

To purify water at low cost for our daily life, the effect of ceramic-based (mullite–cristobalite) and (mullite–zircon) powders doped with different amounts of magnesium oxide (MgO) (10 and 20 wt%) was studied. These compounds are made of a local raw material DD3 with addition of zirconia (ZrO_2) to create an open porosity. The powders were prepared by the traditional mixing method with the help of an automated crushing. The effect of MgO doping on structural, morphological and photocatalytic properties of the material was studied by various analytical techniques such as X-ray diffraction, scanning electron microscopy, energy dispersive X-ray spectroscopy, infrared, and UV–visible spectrometry. The results of XRD proved that there was a deformation in the crystal structure of the two types of ceramics after addition, which resulted in a shift of the spectra to the right, while SEM proved the presence of pores with a larger size as the proportion of MgO increases. The chemical composition of the basic components of the ceramic compounds as well as the additive was confirmed with EDS and IR spectra. The final results show that ceramics with added zirconia (DD3Z) and doped with 10% of MgO have a better photocatalytic efficiency than ceramics without zirconia. This important effect could be related to the higher rate of porosity, which provides a more active surface. The 10% MgO content showed a high photoactivity of 77.33% in only 15 min. The maximum hydrolysis rate obtained with Orange II was 92.95% after a period of 45 min with DD3Z/MgO powders.

Keywords Ceramics/MgO · Photocatalytic · Visible light · Degradation rate

✉ Aleksei Obrosov
aleksei.obrosov@b-tu.de

Mamoun Fellah
mamoun.fellah@yahoo.fr

1. Laboratory of Active Components and Materials, Larbi Ben M'Hidi University, 04000 Oum El Bouaghi, Algeria

2. Mechanical Engineering Department, ABBES Laghrour-Khenchela University, PO 1252, 40004 Khenchela, Algeria

3. MOLTECH-Anjou, Université d'Angers/UMR CNRS 6200, 2 Bd Lavoisier, 49045 Angers, France

4. Department of Physical Metallurgy and Materials Technology, Brandenburg Technical University, 03046 Cottbus, Germany

5. Applied Sciences Department, University of Technology-Iraq, Baghdad, Iraq

1 Introduction

In recent years, the world has experienced strong population growth and industrial modernization [1, 2]. These factors contributed significantly to the percentage of waste that is emitted daily and condenses at the valley and river levels, resulting in a significant increase in their pollution [3–5]. The synthetic dyes used in the textile industry are one of the most dangerous water pollutants, through mixing their turbid waters with the waters of valleys and rivers, and thus lead to environmental disasters affecting humans, animals and plants [6–8].

For the purpose of elimination of these pollutants, local ceramics was used as a catalyst for the final disposal of organic dyes. Kaolin is characterized by a white or gray color depending on the type of impurities or the organic matter present in it and is also easy to break [9]. It is found in nature in the form of very thin hexagonal scales. The materials are produced by the erosion of the bedrock, as most of the kaolin-based materials, are the result of granite deposits with aluminum silicate decomposition and deposition after

transportation by winds and rivers [10]. The chemical formula of pure kaolin is ($Al_2O_3 \cdot 2SiO_2 \cdot 2H_2O$) with an estimated composition of: 39.53% of Al_2O_3, 46.50% of SiO_2, and 13.95% of H_2O [11]. Kaolin is not naturally pure and have impurity percentages varying according to the nature of the materials [12, 13]. Among the three kaolin species, the Algerian local DD3 type was selected with the following impurities MnO, CaO, K_2O, and Fe_2O_3. This material is distinguished by its gray color and mass size of about 2.53 g/cm^3. The chemical analysis of the latter shows that the main component is alumina (Al_2O_3) and (SiO_2) [14].

The application of heterogeneous photocatalysis is one of the most common applications to eliminate the toxicity and contaminants of colored organic dyes, especially Orange II due to its important industrial use [11]. Photocatalysis allows the decomposition of dyes through chemical reactions with the catalysts having the following properties: chemical stability, zero toxicity, and high sensitivity to light [15]. Two types of ceramics: mullite–cristobalite and mullite–zircon (with suitable open porosity rate) were used as basic materials. The first one was extracted from the kaolinite type DD3 and the second one was prepared from the kaolinite type DD3 + 38% ZrO_2 (DD3Z) after heat treatment. The presence of zirconium oxide (ZrO_2) in this clay leads to the formation of zircon ($ZrSiO_4$) with a high degree of open porosity estimated at 33% after consuming the silica in the glass phase [11, 12].

In the goal to increase the efficiency of the decomposition of organic dyes, an oxide with a high catalytic activity was added to the used powders [16]. MgO is one of the semiconductors selected in the study based on its mechanical, electrical, optical and thermal properties that make it a good catalyst for various applications [17–19]. Over the past decades, this material has showed great scientific and technological advantages due to its high thermal stability (up to 2900 °C), low wear resistance, dielectric (dielectric constant 9.8) and large impermeable range (Eg = 7.2 V) [20–22]. Recent studies have also shown that the size and shape of the magnesium oxide nanoparticles give it a high-quality surface as a reaction catalyst, due to structural defects on the surface. It is suitable for water decomposition and hydrogen production [16, 19, 22]. MgO is also used for special wide-ranging biological roles including groundwater, wastewater, drinking water, air emissions and toxic waste treatment, as well as potentially as an antimicrobial agent [16, 21, 23–25].

In this work, the absorption kinetics, the degradation rate of the dye, and the ability of the used catalysts to purify the contaminated dye present in the aqueous solution were studied. These powders were prepared from the traditional mixing method with the help of an automatic crushing. The effect of the percentage of magnesium oxide (MgO) added to the ceramic materials on the photo degradation efficiency was also studied. The obtained results showed that the

degradation of Orange II (OII) has reached 92.95% with the use of powders DD3Z type with addition of 10 wt% MgO, during approximatively 45 min. In the case of powders of pure ceramics DD3, with the same addition (10 wt% MgO) and the same experienced time, a degradation rate of 89.01% was obtained.

2 Experimental study

2.1 Sample preparation equipment

During the preparation process, several devices for sample preparation and thermal treatment were used. To grind the raw materials, a Fritsch crushing device (*Pulverisette 7*) was used. When the powder is placed in the containers of the device, with the addition of distilled water, we add pellets (agate) with a diameter of about 10 mm, which play a major role in obtaining nanometer granules. In the study two electric ovens were used, one of which is used in dehumidification and drying, with a maximum temperature of 220 °C from *Memmert (Schwabach, Germany)*. The second furnace from *Nabertherme* (Lilienthal, Germany) was used for high temperatures (with a maximum temperature of 1350 °C).

2.2 Materials

The primary material used in the production of the ceramic substrates is a local clay of the Djebel Debbagh region (DD3). This raw material was chosen because of its availability in our country, the ease of extraction and good quality [11]. It consists mainly of SiO_2 (51 wt%), Al_2O_3 (47 wt%) and 2 wt% of other oxides. The zirconium oxide (ZrO_2; 99.5% purity) added to these clays is from Sigma–Aldrich.

For the preparation of powders, different percentages of MgO [MgO; 99.0% purity] were added (10, 20%). The photocatalytic test was carried out on an aqueous solution of Orange II ($C_{16}H_{11}N_2NaO_4S$; OII—Sigma–Aldrich).

2.3 Preparation of the DD3/ZrO$_2$ kaolin mixture

After the treatment at 1300 °C two types of ceramic powders were used in this study. The first one consists mainly in mullite and cristobalite and the other one in mullite and zircon. These powders are without zirconia (DD3) or with the addition of zirconia (DD3 + 38% ZrO_2). The choice of this raw material is justified by the fact that ceramics are

available in a significant quantity in nature, and in Algeria in particular.

The region of its extraction is Djebel Debbagh, located in Guelma (36° 31′ 52 N and 7° 16′ 03). This site is characterized by a ceramic rich in kaolinite clay of various types. The addition of 38 wt% of zirconia (ZrO_2) is justified by the goal to fabricate zirconium silicate ($ZrSiO_4$) with the SiO_2 compound remaining from the kaolinite ceramics [26, 27].

2.4 Methods of MgO-doped ceramics powders

The traditional mixing method is easy, quick to perform and less expensive than other methods. Moreover, it is the most used methods to obtain solid solutions based on the reaction of a mixture of oxides inside an agate vessel using automatic crushing. [19–21]. This technique is mainly based on the easy and short time of the fabrication process and the use of less expensive compounds.

Ceramic powders and MgO oxide with specified ratios were mixed and ground using a grinder. Figure 1 presents the different steps of the preparation of the mixture by the traditional method. We note that these steps are the same for all mixtures; the difference is in the amount of oxide added to the different ceramic materials.

For the fabrication, 1 g of ceramic powders (DD3 or DD3 + 38% ZrO_2) without or with the addition of magnesium oxide (10 and 20%) were placed in containers with the addition of 20 ml of distilled water. Seven grains

(agate) with a diameter of about 10 mm were added, which contributes to obtaining particles of nanometer sizes. An automatic grinder machine was used at a rotational speed of $V = 200$ °C/min for 5 min. The prepared powders were dried in an oven at 200 °C for 30 min. In the last step the prepared powders were treated for two hours at 500 degrees to obtain crystallized materials and to enable the removal of residual organic compounds by oxidation during processing at high temperatures (> 300 °C). Thus, the prepared ceramic-based powders are used as catalysts. The process steps are shown in Fig. 1.

2.5 Characterization techniques

The crystal structure of the powder particles was identified by X-ray diffraction (Bruker AXS-8 D) using a type of radiation CuKα ($\lambda = 1.5406$ Å).

For scans on JOIDES Resolution, the randomly oriented bulk powders were top mounted onto sample holders and scanned using a Bruker AXS-8D Endeavor diffractometer mounted with a VANTEC-1 detector and nickel-filtered CuKα radiation. The routine locked-coupled scanning parameters were set as follows: Voltage = 40 kV. Current = 30 mA. Goniometer angle $2\theta = 15°$–$45°$, Step size = 0.02°, Scan speed = 0.5 s/step, and Divergence slit = 0.6 mm.

The raw digital data processed on JOIDES Resolution using the DIFFRAC.EVA software package, which allows for baseline definition (set at enhanced, 1.000 curvature, and 1.000 threshold) and smoothing (set at smooth default factor = 0.124). Diagnostic net peak areas (recorded in units of counts/s × angle [in 2θ], measured above the baseline) for each mineral (or mineral group) were determined using the "create area" function in DIFFRAC.EVA; that function accommodates manual adjustment of the upper and lower limits of the peaks.

The FTIR spectroscopy is a physical process which is based on the interactions of infrared radiation (electromagnetic radiation with wavelengths of approx. 0.7–500 μm) with matter. In the identification of unknown substances, infrared spectroscopy represents a quantitative method of frequent application.

The vibrational spectra for all samples were obtained using a Bruker II-RAM spectrometer, equipped with an infrared source, potassium bromide beam splitter, and high sensitive DigiTectTM detector system. Disks of 13 mm diameter and 2 mm thickness, consisting of approximately 0.6 mg sample gently dispersed in 200 mg of KBr, were carefully heated at 120 °C to minimize the amount of the absorbed water. Disks were then immediately and thoroughly scanned in the wavenumber region of 400–4000 cm^{-1} in transmission mode with a resolution of 4 cm^{-1} with 128 successive scans.
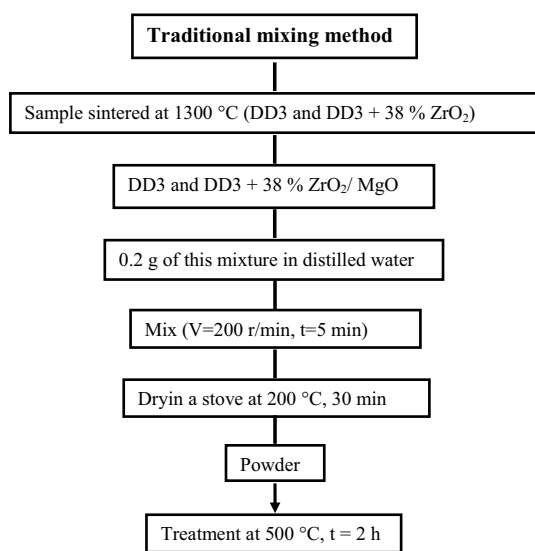

Fig. 1 Preparation of powders using traditional mixing

A scanning electron microscope (JSM-6301F) was used to explore the different regions of the samples and to perform an elemental chemical analysis using an Energy-Dispersive X-ray spectrometer (EDX-X-Max 20 mm^2). The elemental and chemical compositions of the prepared powders were characterized by Infrared (IR) spectroscopy (Bruker II-RAM).

2.6 Measurement of photocatalytic activity

The photocatalytic activity of various pellets and powders were monitored by means of a UV spectrometer (V-630, JASCO) in the goal to measure the absorbance with a wavelength range of 250–650 nm. Orange Dye II (OII) was selected as an organic substrate for catalyst tests to evaluate the effects of the powders. The colored aqueous solutions were prepared from orange II by dissolving a quantity of dye in distilled water and stirring with a magnetic mixer for half an hour to completely dissolve the dye.

0.2 g of powder with different MgO additives (10 and 20 wt%) in 25 ml of aqueous OII solution (25 mg/l, PH 8.9) was used. After each period of 15 min, 2.2 ml of a solution was taken, then centrifuged at 3500 U/min for 7 min to separate the solid part from the liquid. Finally, the resulting solution was analyzed by absorbance spectra in the wavelength range 250–650 nm. After each optical measurement, the absorbance spectra were measured. The rate of decomposition and degradation of the colored solution was calculated using the following relationship [11, 27, 28]:

$$\text{Degradation (\%)} = \frac{C_0 - C}{C_0} \times 100, \tag{1}$$

where C_0 represents the initial concentration of the solution before placing the catalyst, whereas C represents the varying concentration of the solution during each measurement.

3 Results and discussion

3.1 X-ray diffraction

The powders produced by different percentages of magnesium oxide (10, 20 wt%) were treated at 500 °C and characterized by X-ray diffraction (XRD). The obtained results are shown in Fig. 1a–f. Figure 1a, b presents DD3 ceramic powders prepared by a traditional mix method. In addition to the peaks of the ceramic phases: mullite with $2\theta = 16.36°$, 25.86°, 26.27°, 31.02°, 33.20°, 35.23°, 37°, 39.30°, 40.94°, and 42.57° (JCPDS 15-0776), zircon with $2\theta = 20.01$, 26.99, 35.64, 38.55, and 43.83° (JCPDS 06-0266), Mono crystalline zirconia (ZrO$_2$) at $2\theta = 17.48$, 24.13, 24.45, 28.20, 31.48, 33.85, and 34.17° (JCPDS 37-1484), and cristobalite with $2\theta = 21.66°$ and 35.78 (JCPDS 39-1425)) [11, 26, 27].

The addition of MgO contributes to a change in the lattice parameters which results in a slight shift of the peaks. The higher MgO content in the powder, the greater the shift to the right is observed. This leads to a deformation of the crystal structure due to the expansion of the cell and changes in its dimensions due to the occupation by large Mg atoms (Mg^{2+} = 0.72 Å) sites in the ceramic (Al^{3+} = 0.5 Å, Si^{4+} = 0.40 Å)) [11, 22]. As shown in Table 1, the size of the granules increases with the addition of the MgO in case of mullite–cristobalite from 27.2 to 34.5 nm. It is also observed that with the increasing of magnesium oxide content in the powder, a low intensity peak at 18.11° appears, which characterizes Mg(OH)$_2$ (Fig. 2e) [20].

In Fig. 2f (DD3 + 38 wt% ZrO$_2$ + 20 wt% MgO), the observed peaks were attributed to the MgO phase corresponding to the (200) plane. The addition of 20 wt% of MgO leads to an increase of the intensity of the mullite, zirconium, and cristobalite phases, which becomes more crystallized and decreases in the zircon phase when 10 wt% of MgO is added (Table 2). There is a clear decrease in all of the peaks by increasing the proportion of magnesium oxide to 20 wt% in the ceramics powders for the two parameters (the width of the lines decreases, and the size of the granules increases). The peak (200) of the magnesium oxide phase is shown in the diffraction spectrum (DD3 + 38% ZrO$_2$ (80%) + MgO) at

Table 1 Results of structural analysis type DD3 before and after MgO addition

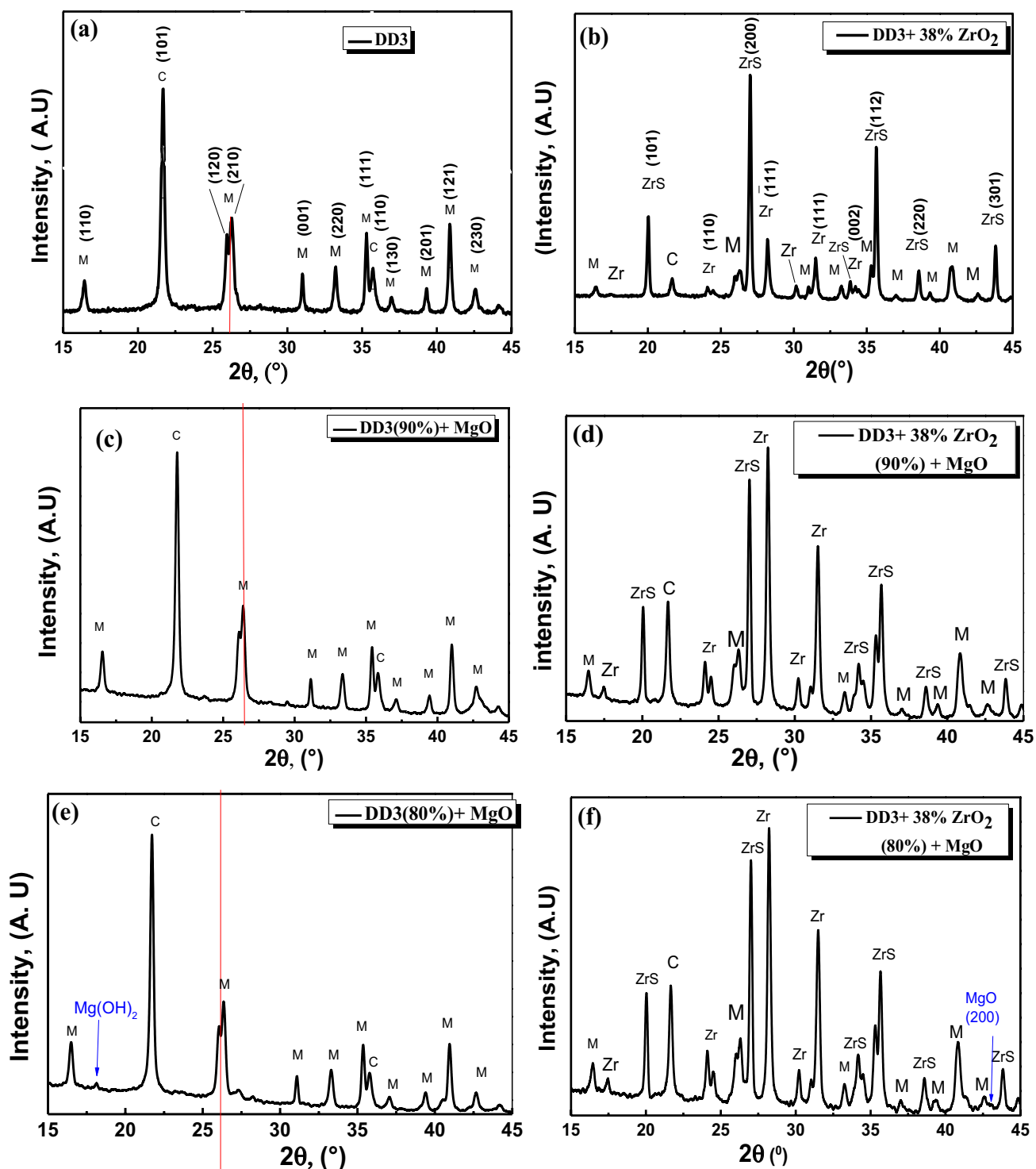| Phases	Plan (hkl)	2Θ (°)	Θ (°)	FHWM β (°)	B (rad)	D (nm)
Mullite	(210)	26.28	13.14	0.356	0.0062	23.0
Mullite + 10% MgO	(210)	26.4	13.20	0.302	0.0053	26.9
Mullite + 20% MgO	(210)	26.45	13.23	0.316	0.0055	25.9
Cristobalite	(101)	21.68	10.84	0.261	0.0045	31.4
Cristobalite + 10% MgO	(101)	21.78	10.89	0.259	0.0045	42.1
Cristobalite + 20% MgO	(101)	21.72	10.86	0.26	0.0045	31.4

Fig. 2 X-ray scattering scheme of DD3 and DD3 + 38% ZrO$_2$ powders with 10 wt% and 20 wt% MgO, treated at 500 °C for 2 h. *ZrS* zircon, *Zr* zirconia, *C* cristobalite, *M* mullite. **a** DD3, **b** DD3 + 38 wt% ZrO$_2$, **c** DD3 + 10 wt% MgO, **d** DD3 + 38 wt% ZrO$_2$ + 10 wt% MgO, **e** DD3 + 20 wt% MgO, **f** DD3 + 38 wt% ZrO$_2$ + 20 wt% MgO

42.96° with a low intensity due to the used treatment temperature value, or its formation in small quantities, which is not explained by the X-ray diffraction technique.

3.2 Scanning electron microscopy (SEM)

The morphology of the catalyst was studied by SEM, where

Table 2 Results of structural analyzes of type DD3 + 38% ZrO_2 before and after the MgO addition

Phases	Plan (hkl)	2Θ (°)	Θ (°)	FHWM β (°)	β (rad)	D (nm)
Mullite	(121)	40.82	20.41	0.382	0.0067	22.1
Mullite + 10% MgO	(121)	40.84	20.42	0.383	0.0067	22.2
Mullite + 20% MgO	(121)	40.84	20.42	0.346	0.0060	24.6
$ZrSiO_4$	(200)	27.02	13.51	0.188	0.0033	43.2
$ZrSiO_4$ + 10% MgO	(200)	27.01	13.51	0.247	0.0043	33.1
$ZrSiO_4$ + 20% MgO	(200)	27.03	13.52	0.159	0.0028	50.9
ZrO_2	(−111)	28.20	14.1	0.209	0.0036	39.7
ZrO_2 + 10% MgO	(−111)	28.23	14.11	0.295	0.0051	28.0
ZrO_2 + 20% MgO	(−111)	28.24	14.12	0.189	0.0033	43.3
SiO_2	(101)	21.67	10.83	0.246	0.0043	32.8
SiO_2 + 10% MgO	(101)	21.69	10.84	0.248	0.0043	32.8
SiO_2 + 20% MgO	(101)	21.67	10.83	0.237	0.0041	34.4
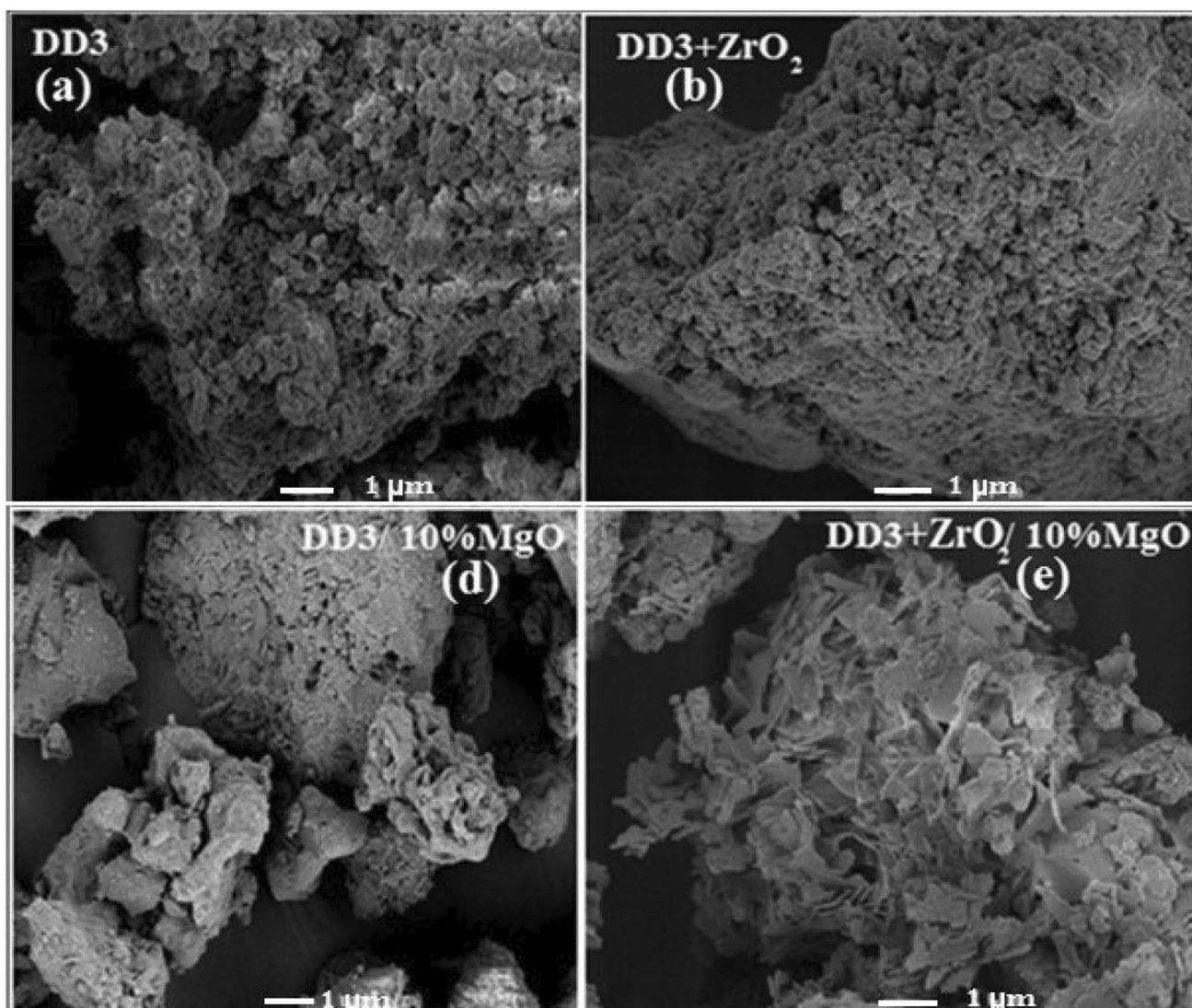
Fig. 3 SEM images of powders before and after addition of MgO: **a** DD3, **b** DD3 + ZrO_2, **c** DD3/10 wt% MgO, **d** DD3 + ZrO_2/10 wt% MgO
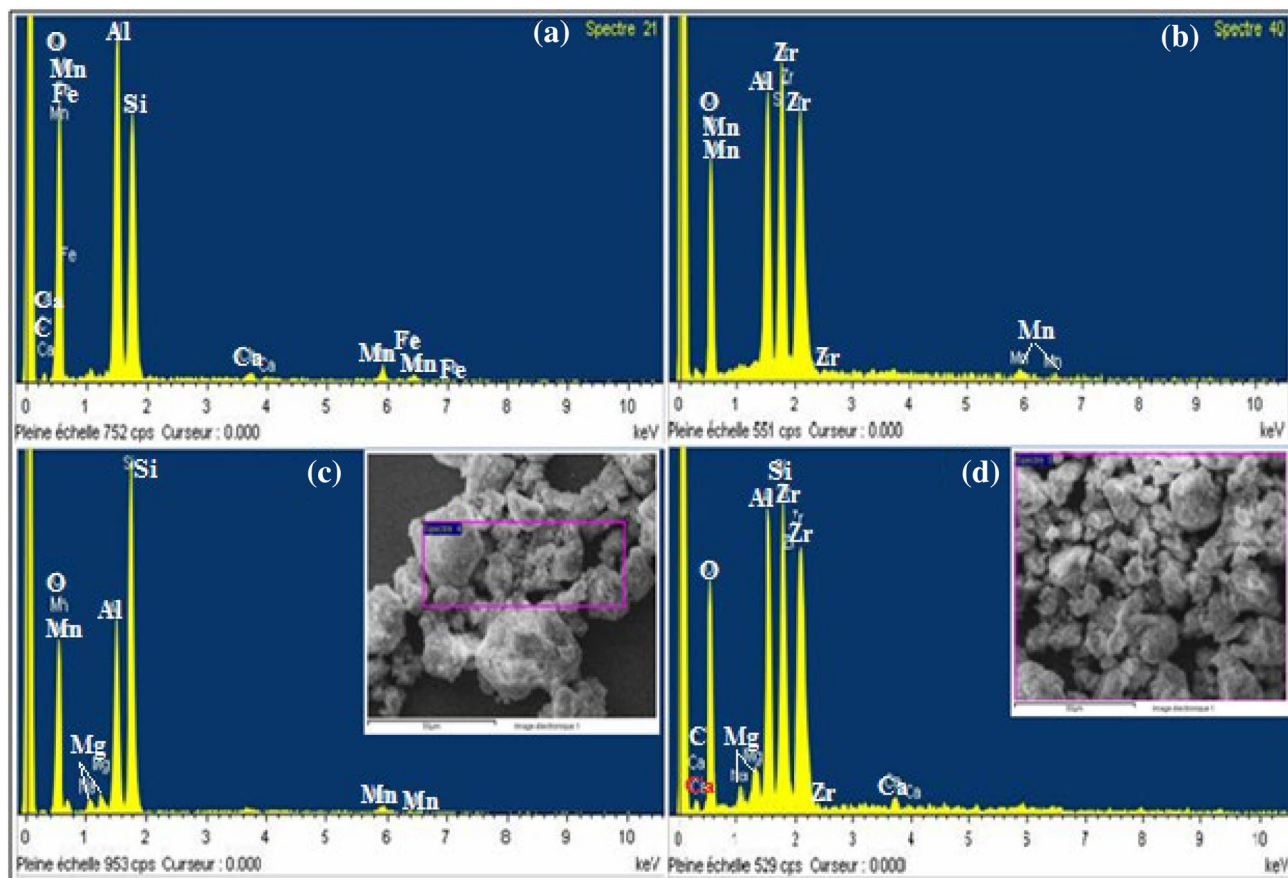
Fig. 4 EDX spectra for the powders before and after the addition of MgO: **a** DD3, **b** DD3 + ZrO$_2$, **c** DD3/10 wt% MgO, **d** DD3 + ZrO$_2$/10 wt% MgO

the grain size was not homogeneous due to the difference in particle sizes of ceramic materials and additives. Figure 3a, b shows a clear change in the granule shape after addition of zirconium oxide to DD3. It is also noticeable that the pore ratio increases, where the average pore size reaches 292.5 nm compared to 50.2 nm without addition. The addition of 10% MgO to both types of ceramics significantly increased the percentage of pores within the granule, resulting in more active materials for better photocatalytic efficiency and the specific application used in this work.

MgO contributes to change the morphology of the DD3Z type. A compact flake (chips) structure (Fig. 3d) is observed, making them more porous compared to the DD3 type (Fig. 3c), which keeps the same shape with an increase of the open porosity fraction. As a result, the addition of magnesium oxide made a significant contribution to the porous structure and is ideal for photocatalysis applications.

3.3 Energy dispersive X-ray spectrometry

The chemical composition of the powders was examined after a heat treatment at 500 °C for 2 h by EDX analysis (Fig. 4). From the spectra, the atomic percentages of the main elements present for the ceramics (O, Al, Si, Zr) were extracted. Table 3 shows the percentage of main chemical

Table 3 Quantitative analysis of the EDX spectra of the powders prepared by the mixing method

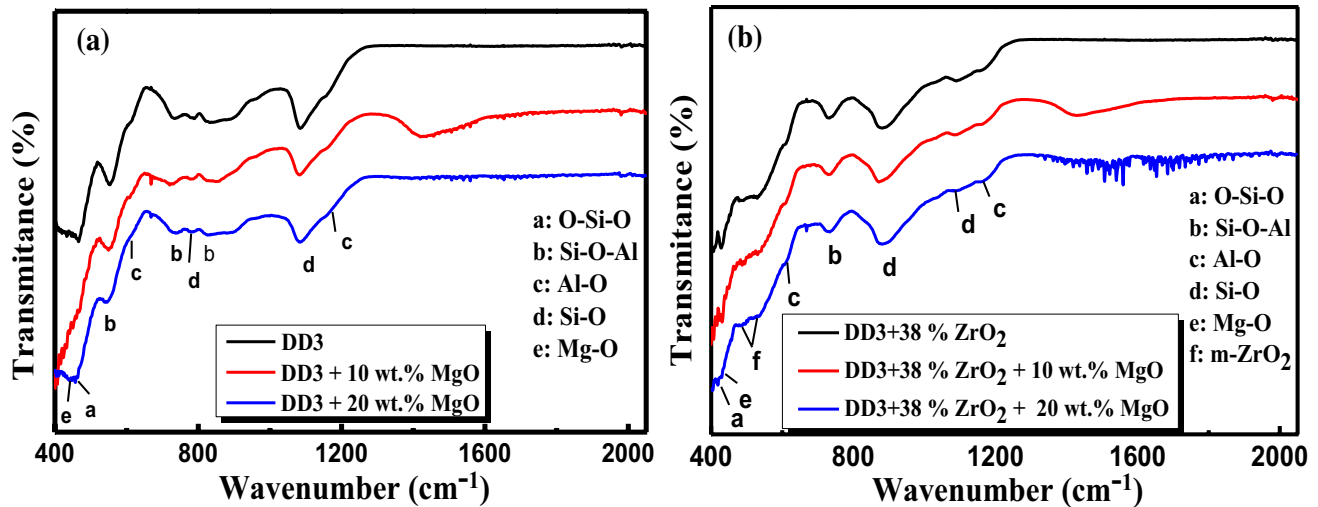| Powders	Elements, at%					
	O (%)	Mn (%)	Mg (%)	Zr (%)	Si (%)	Al (%)
DD3	63.35	4.23	–	–	13.99	14.8
DD3Z	61.93	2.81	–	4.24	12.29	14.51
DD3/MgO	62.61	0.58	0.97	–	23.71	10.83
DD3Z/MgO	70.72	–	0.09	5.75	13.62	10

Fig. 5 IR spectra of powders prepared without and with the addition of different percentages of MgO treated at 500 °C for 2 h

elements. Most of the substrate components (Si, Al, and Zr) are similar and reasonable, while the additive components (Mg) are weaker. The main percentage of compounds is Si, since the amount of its presence in ceramics is the largest.

Based on these spectra, the presence of magnesium was found at a very low percentage. This result is due to the percentage of the Mg added to the ceramic powders and confirms the doping of specific DD3 and DD3Z ceramics with magnesium oxide.

3.4 Infrared (IR) spectra

To obtain a better characterization of the chemical sample compositions and interactions affecting the sample properties, the IR technique was used for the characterization of the obtained powders. This technique is frequently used to study structures, compositions, and chemical properties of materials. The obtained results by IR spectroscopy are presented in Fig. 4. Several absorption bands in the wavelength range, from 400 to 2000 cm^{-1}, are clearly identified.

Figure 5 shows the infrared spectra of ceramic powders without and with the addition of different percentages of MgO by the traditional mixing method at 500 °C for 2 h. Seven absorption peaks in both compounds are observed at 615, 735, 1086, and 1159 cm^{-1}. They are related to the process of forming the mullite present among them [11]. By comparing these results with the results obtained in the literature, the absorption bands at 615 and 1159 cm^{-1} are assigned to vibrations of the Al–O bond, while the 1086 cm^{-1} represents the Si–O bond. One can additionally notice that the appearance of the absorption band at 466 cm^{-1} characterizes O–Si–O bending vibrations (ν_2) [28]. Three absorption lines at 553, 735, and 834 cm^{-1}
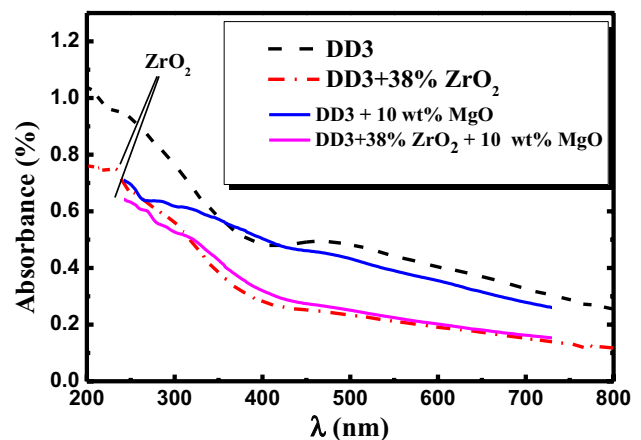

Fig. 6 UV–visible absorption spectra of the catalysts

have a special association with Si–O–Al [29]. The cristobalite was assigned to an S–O stretching, appearing at 788 cm^{-1} value [30]. The reduction in the spectrum value was observed with the addition of zirconium oxide and is increased at 885 cm^{-1}. However, in this special case of the SiO$_4$ group (ν_3), the presence of the ZrSiO$_4$ phase is observed [11]. The IR spectrum shows the absorption band at 420 cm^{-1} characteristics of the MgO phase after addition of 10 wt% of the latter. The effect of MgO addition to the mixing method was demonstrated by the appearance of the Mg–O absorption band at 420 cm^{-1} after addition of 10 wt% MgO. It is observed that the spectrum is clearly changed in the range [400–500] cm^{-1} and no characteristic band of an additional phase is shown. The addition at 20 wt. % of MgO was confirmed by the appearance of an absorption band at 419 and 486 cm^{-1} of the Mg–O vibration mode [27, 28]. An absorption band characteristic of

–OH is due to the harmonic vibrations of H_2O [29–31] and observed for DD3 + 38% of ZrO_2.
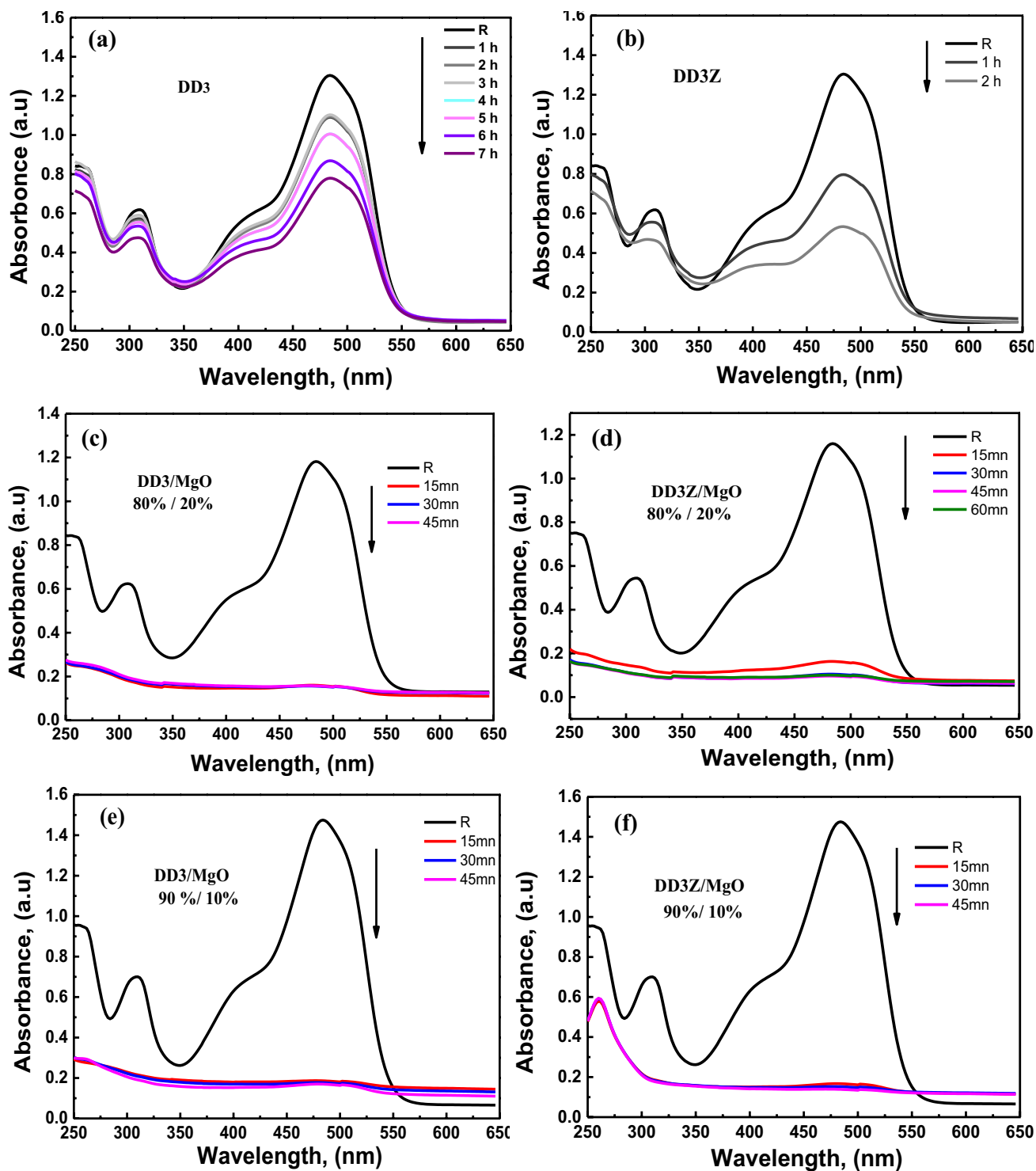

Fig. 7 Absorption spectra showing the effect of the mixture preparation method of ceramic powders doped with different percentages of MgO, with a treatment at 500 °C for the degradation of OII ($\lambda_{max} = 484$ nm): **a** DD3, **b** DD3 + 38%ZrO_2, **c** DD3 (80%)/MgO, **d** DD3 + 38% ZrO_2(80%)/MgO, **e** and **g** DD3(90%)/MgO, **f** and **h** DD3 + 38% ZrO_2(90%)/MgO

3.5 Optical analysis

Figure 6 shows the results of the optical analysis performed for DD3, DD3 + 38 wt% ZrO_2 and DD3/DD3 + 38 wt% ZrO_2 + 10 wt% MgO powders. The measurements were performed in the wavelength range of 200–800 nm. It can be noted in the latter case that the absorbance decreases for sample DD3 + 38 wt% ZrO_2. Thus, the addition of ZrO_2 to the DD3 clay plays an opposite role in the absorbance compared to the photocatalytic degradation. The absorbance decrease with the addition of ZrO_2 in the clay can be explained by the formation of $ZrSiO_4$ component characterized by a great optical reflection of the grains [32].

Consequently, the presence of MgO in the DD3 and DD3 + 38 wt% ZrO_2 clay improves the absorbance in a remarkable way. An increase of the photocatalytic effect is attributed to the increase of the reaction surface (grain porosity). Zirconium oxide (ZrO_2) absorbs at 233 nm. After the addition of 10 wt% of MgO to the two types of ceramic materials, the absorbance is increased.

3.6 Photocatalytic performance

As shown by the absorbance spectra obtained when the prepared materials are exposed to visible light. MgO provided a high efficiency in the analysis of solutions contaminated with OII. Figure 7 shows the absorbance spectra prepared by mixing in the grinder two types of ceramics (DD3 and DDZ) without and with various amount of MgO and subjected to visible light. The OII degradation rate of ceramic powders without MgO addition was 42.0%
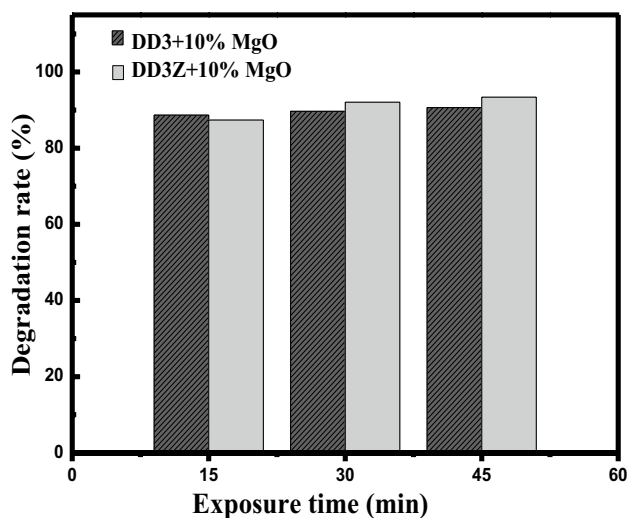

Fig. 8 Degradation rate of Orange II versus UV exposure time for DD3 and DD3 + 38% ZrO_2 with 10 wt% of MgO

for DD3 (Fig. 7a) and 60.3% for DD3Z (Fig. 7b), during periods of 7 and 2 h, respectively. These values are significantly improved with an increase of the MgO percentages (Fig. 7c–f), where the purification degree reached higher values in shorter time periods.

The best purification was obtained with a value of 92.95% for DD3Z (Fig. 7f), whereas 89.01% was obtained for the second DD3 type (Fig. 7e) for OII within 45 min when 10 wt% of MgO was added. The best results were obtained when 10% of MgO was added. The figure and 7 h present the results of photocatalysis for the titration of the solution every 5 min instead of 15 min. With the same addition of magnesium oxide (10 wt%), the degradation rate of OII reached 77.33% for DD3Z type and 74.13% for DD3 type within 5 min (Fig. 7g, h).

Both types of ceramic material without MgO addition are not effective for photocatalysis and the difference appear only after several hours. With an addition of MgO, the catalyst occurs very quickly, and the transparency of the solution appears just a few minutes after adding the catalyst materials (Fig. 8).

3.7 Photocatalytic principle

Photocatalysis is an advanced oxidation or reduction process that catalyzes by excitation of the electronic space through the excited chemical reaction resulting in absorption of a photon. The semiconductor can be considered as a catalyst. The principle of photocatalysis is close to the heterogeneous catalyst where the oxidation-reaction takes place at the surface of the semiconductor.

Inhomogeneous photodynamics depends on the generation of pairs (holes/electrons) in semiconductors by absorbing photons whose energy is equal to or greater than the bandgap energy (hv ≥ Eg) (Eq. 2) [33]. After photon absorption and the formation of (e^-/h^+) pairs in the bulk of the solid it appears: either the recombination by the release of heat, or the interaction with the species absorbed on the surface of the semiconductors [33–35]. These pairs of electrons/holes are separated into free electrons in the conduction band and holes in the valence band. This phase will freeze its activity. At the same time, the presence of the fluid phase (gas or liquid) produces automatic absorption depending on the redox potential (or energy level) by transferring the electron towards the acceptor molecules (A) (Eq. 3), whereas the holes are transferred to the donor molecules (D) (Eq. 4). This phenomenon results in the production of very effective free radicals resulting in the return of oxygen and oxidation of water according to Eqs. (5, 6).

The production of hydroxyl radicals (•OH), is very effective during photocatalysis. These radicals reduce the proportion of any chemical compound and decompose it to have a high oxidation capacity (2.8 eV) compared to other oxidants such as

O_2 (2.42 eV) and H_2O_2 (1.78 eV) [30]. Other oxidizing types such as OH and H_2O_2 can also appear and lead to the formation of an intermediate product and possibly to the mineralization of the chemical compounds absorbed on the surface of the photocatalyst. The described processes are summarized by the following chemical equations:

$$h\nu + (SC) \rightarrow h^+ + e^-, \tag{2}$$

$$A(ads) + e^- \rightarrow A^-(ads), \tag{3}$$

$$D(ads) + h^+ \rightarrow D^+(ads), \tag{4}$$

$$H_2O + h^+ \rightarrow \bullet OH + H^+, \tag{5}$$

$$O_2 + e^- \rightarrow \bullet O_2^- + 4H^+. \tag{6}$$

3.8 Powder mechanism (DD3Z/MgO)

The tested samples for photocatalysis are based on ceramic materials of types DD3 and DD3Z with the addition of MgO. In the presence of zirconium oxide in the ceramics, hydroxyl roots (radicals) of •OH are formed. For this phenomenon, a pair (e^-/h^+) must be created in the semiconductor by absorbing a photon with an energy equal to or greater than the energy gap. These pairs are separated by Al_2O_3 molecules [30, 36], •OH radicals simultaneously act on the surface areas of the contaminant adsorbed on SiO_2 and Al_2O_3 [30].

However, this degradation is unsatisfactory as shown by Eqs. 9, 11, 13, 15 and 20 [37, 38]. After the addition of MgO, a significant improvement was obtained, providing excellent efficiency and acceleration of the photocatalysis process for OII analysis in a quick time (approximately

5 min). These results are good even without the presence of zirconium oxide and despite the large gap energy compared to previously used oxides. The diagram shown in Fig. 9 represents the mechanism of photocatalysis by a visible light. After sufficient energy absorption, it was possible to create the e^-/h^+ pairs by the two oxides (MgO, ZrO_2). These electrons are separated, moving from a larger band to a lower one.

As a result, the conduction band of MgO is higher than the conduction band for ZrO_2, and, therefore, there may be a rapid transfer of electrons formed in the conduction band (C B) at MgO to the CB for ZrO_2(this prevents recombination) [39–41]. The CB edge potentials of MgO ($- 3.20$ eV) and ZrO_2 ($- 0.88$ eV) are negative compared to the standard redox potential $E\Theta(O_2/\bullet O)$ ($- 0.33$ eV vs. NHE) [32, 41]. Therefore, the electrons for MgO and ZrO_2 can reduce O_2 to $\bullet$ O (Eqs. 9, 10).

The mechanism then begins again, where holes (h^+) interact with the water (H_2O) to produce the hydroxide OH, and contributes to the photocatalysis of the colored material. Electrons (e^-) react with O_2giving the contaminated solution a white color (Eqs. 11, 12, 13, 14) [32, 42–44] • O can interact with H_2O to form HO and H_2O_2, as shown in Eqs. (19, 20, 21). Due to the position of the VB (valence band) edge for ZrO_2 and MgO ($+ 4.6$ eV for MgO and $+ 3.22$ eV for ZrO_2) there is a possibility of oxidation of the dye to carbon dioxide (CO_2) and water (H_2O) with magnesium oxide and zirconium oxide through the holes mentioned above (Eqs. 20).

The reaction of the oxidants ZrO_2 and MgO increases the • OH level in a very noticeable way compared to the presence of zirconium oxide alone in the ceramics. Hole (h^+) formation is also based on the chemical nature of these oxides, which may explain the increased rate of OII degradation in powders mainly forming DD3 ceramics with ZrO_2 and MgO compared to other cases. The chemical equations are:
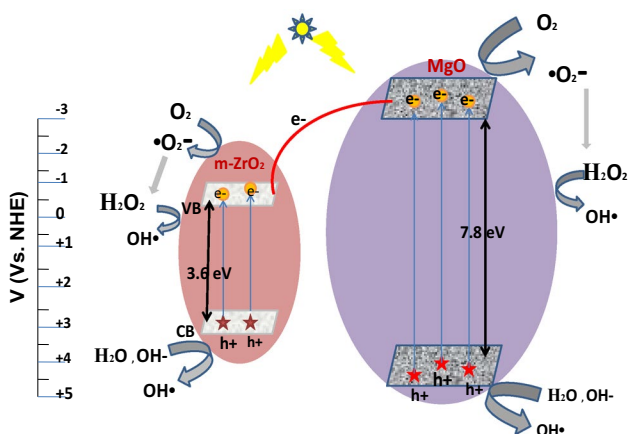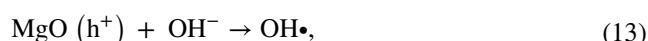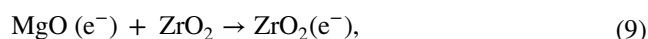
$$ZrO_2 + h\nu \rightarrow ZrO_2(e^-) + ZrO_2(h^+), \tag{7}$$

$$MgO + h\nu \rightarrow MgO(e^-) + MgO(h^+), \tag{8}$$

$$MgO(e^-) + ZrO_2 \rightarrow ZrO_2(e^-), \tag{9}$$

$$ZrO_2(e^-) + O_2 \rightarrow \bullet O_2^-, \tag{10}$$

$$MgO(e^-) + O_2 \rightarrow \bullet O_2^-, \tag{11}$$

$$ZrO_2(h^+) + OH^- \rightarrow OH\bullet, \tag{12}$$

$$MgO(h^+) + OH^- \rightarrow OH\bullet, \tag{13}$$
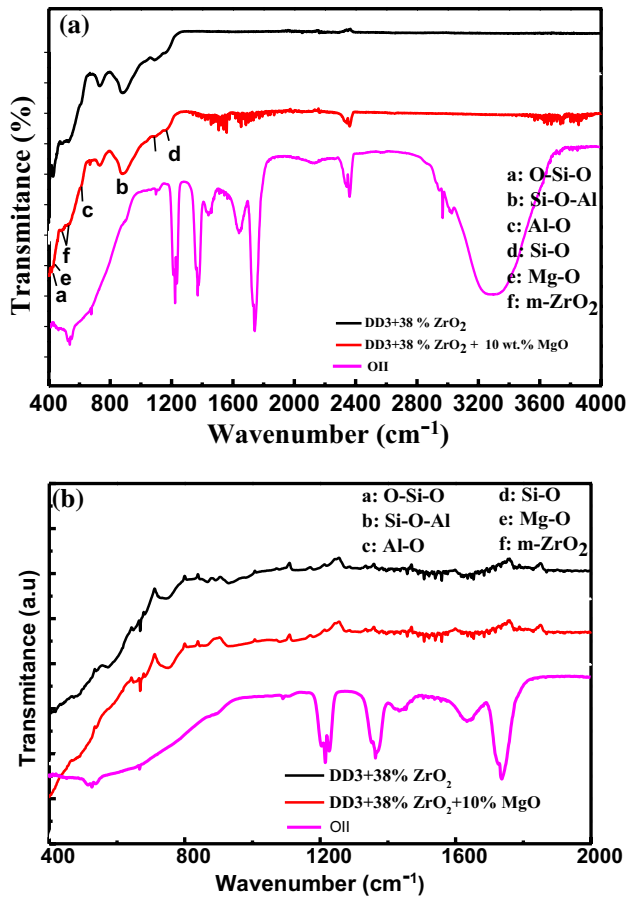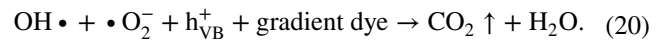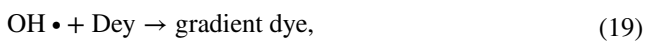

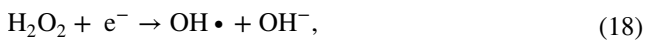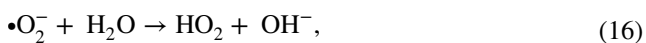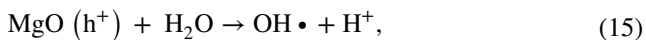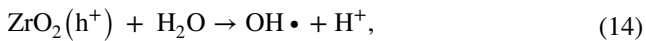**Fig. 9** Mechanism of photocatalysis for the compound ZrO_2/MgO

Fig. 10 Infrared absorption spectrum of the catalytic powder after photocatalysis, **a** [400–4000] cm^{-1} and **b** [400–2000] cm^{-1}

$$OH \bullet + \bullet O_2^- + h_{VB}^+ + \text{gradient dye} \rightarrow CO_2 \uparrow + H_2O. \quad (20)$$

3.9 Study of adsorption by infrared spectroscopy

To conclude whether or not the OII particles were adsorbed on the surface of the catalyzed powders, the samples were analyzed after photocatalysis by infrared spectroscopy. The powder of type DD3Z was selected with 10% added percentage of MgO, which was studied in the frequency range [400–4000] cm^{-1}. The obtained spectra are shown in Fig. 10b where they indicate the presence of the same absorption peaks mentioned above, but less clear at 466, 553, 740, 840, 1160 cm^{-1} [30], proportional to the vibrations of the bonds of type O, Al, Si, Zr of various kinds. As for MgO, absorbance peaks appear at 420 cm^{-1} [22]. What is new is the presence of oscillations on the spectra after the end of the photocatalytic process.

Also it is noted the complete absence of peaks of the organic pollutant OII by comparing the absorption spectra of the powders after photocatalysis and the spectrum of the organic compound Orange II (Fig. 10a), which indicates its decomposition and thus the effectiveness of these powders in the purification of polluted water.

4 Conclusions

Two different types of kaolinite, DD3 and DD3Z, with common mineral-based phyllosilicate, are used to remove organic pigments from water.

- After adding magnesium oxide to the ceramic material, X-ray analysis showed spectra shifts towards larger angles. This is due to the occurrence of deformation and compression in the crystal lattice of the ceramic after doping.
- It was found that with a higher percentage of MgO, an increase in the size of the particles is observed. We characterize the morphology of the prepared powders using SEM.
- It was found that the addition of 10% by weight of MgO to ceramics of the type (DD3 + ZrO2) contributed to the change in the shape of the particles, which led to the formation of a compact flake structure. The addition was confirmed by EDX analyzes, which confirmed the presence of Mg and O elements in both species.
- The photocatalytic activity of the prepared samples had a significant effect on the decomposition of Orange II dye under visible light.

$$ZrO_2(h^+) + H_2O \rightarrow OH \bullet + H^+, \quad (14)$$

$$MgO(h^+) + H_2O \rightarrow OH \bullet + H^+, \quad (15)$$

$$\bullet O_2^- + H_2O \rightarrow HO_2 + OH^-, \quad (16)$$

$$2HO_2 \rightarrow H_2O_2 + O_2, \quad (17)$$

$$H_2O_2 + e^- \rightarrow OH \bullet + OH^-, \quad (18)$$

$$OH \bullet + Dey \rightarrow \text{gradient dye}, \quad (19)$$

– OII degradation was obtained 5 min after the start of the process. The efficiency was estimated to 77.33% for DD3Z type and 74.13% for DD3 type.

– These results allow the development of photocatalysts from natural and neutral local material. The degradation rate increases to 89.01% for DD3 and 92.95% for DD3Z when 10% by weight of MgO is added with the same exposure time of 45 min.

Data availability Not applicable for that section.

Code availability Not applicable for that section.

Declarations

Conflict of interest The authors have no relevant financial or non-financial interests to disclose.

Ethical approval Not applicable for that section.

Consent to participate Not applicable for that section.

Consent for publication Not applicable for that section.

References

1. R.R. Chen, Q.F. Ren, Y.X. Liu, Y. Ding, H.T. Zhu, C.Y. Xiong, W.C. Oh, J. Korean. Ceram. Soc. **58**(5), 548–558 (2021)
2. L. Zhu, Y. Dong, S. Hampshire, S. Cerneaux, L. Winnubst, J. Eur. Ceram. Soc. **35**, 711–721 (2015). https://doi.org/10.1016/j.jeurceramsoc.2014.09.016
3. J. You, Y. Guo, R. Guo, X. Liu, Chem. Eng. J. **373**, 624–641 (2019)
4. D. Schultz, T. Yoon, Science **48**, 1239176 (2019)
5. A. Noypha, Y. Areerob, S. Chanthai, P. Nuengmatcha, J. Korean. Ceram. Soc. **58**(3), 297–306 (2021)
6. M.-H. Sun, S.-Z. Huang, L.-H. Chen, Y. Li, X.-Y. Yang, Z.-Y. Yuan, B.-L. Su, Chem. Soc. Rev. **45**, 3479–3563 (2016). https://doi.org/10.1039/C6CS00135A
7. M. Fellah, N. Hezil, R. Djellabi, M. Abdul Samad, M.Z. Touhami, A. Montagne, A. Iost, Appl. Clay Sci. **177**, 43–50 (2019)
8. E. Ersöz, Y.O. Altintas, J. Korean Ceram. Soc. 1–16 (1) (2022)
9. A.E. Oksuz, M. Yurddaskal, M. Erol, J. Korean Ceram. Soc. **14**, 1–9 (2022)
10. S. Das, V.C. Srivastava, Nanotechnol. Rev. **7**, 267–282 (2018). https://doi.org/10.1515/ntrev-2017-0144
11. D. Bouras, A. Mecif, R. Barille, A. Harabi, M. Zaabat, Ceram. Int. **46**, 20838–20846 (2020). https://doi.org/10.1016/j.ceramint.2020.05.114
12. A. Mecif, J. Soro, A. Harabi, J.P. Bonnet, J. Am. Ceram. Soc. **93**(5), 1306–1312 (2010). https://doi.org/10.1111/j.1551-2916.2009.03595.x
13. H. Senoussia, C. Osmania, M. Courtoisb, M.H. Bourahli, Bol. Soc. Espanola Ceram. Vidr. **5**, 121–126 (2016). https://doi.org/10.1016/j.bsecv.2015.12.001
14. Y.H. Yun, J.K. Lee, J. Korean Ceram. Soc. **59**(3), 393–400 (2022). https://doi.org/10.1007/s43207-021-00180-y
15. S. Bouzid Rekik, J. Bouaziz, A. Deratani, S. Baklouti, Period Polytech. Chem. Eng. **61**, 206–215 (2017). https://doi.org/10.3311/PPch.9679
16. N. Salehifar, Z. Zarghami, M. Ramezani, Mater. Lett. **167**, 226–229 (2016). https://doi.org/10.1016/j.matlet.2016.01.015MLBLUE20143
17. L. Chen, C. Xu, X.F. Zhang, T. Zhou, Physica E. **41**, 852–855 (2009). https://doi.org/10.1016/j.physe.2009.01.006
18. M.R. Anilkumar, H.P. Nagaswarupa, H. Nagabhushana, S.C. Sharma, Y.S. Vidya, K.S. Anantharaju, Spectrochim. Acta Part A Mol. Biomol. Spectrosc. **149**, 703–713 (2015). https://doi.org/10.1016/j.saa.2015.05.003
19. P. Tamilselvi, M. Hema, R. Anbarasan, Nano Bullet. **1**, 130–106 (2013). https://doi.org/10.1234/NANO130106
20. K. Krishnamoorthy, G. Manivannan, S.J. Kim, K. Jeyasubramanian, M. Premanathan, J. Nanopart. Res. **14**, 1063 (2012). https://doi.org/10.1007/s11051-012-1063-6
21. M. Part, A. Tamm, J. Kozlova, H. Mändar, T. Tätte, K. Kukli, Thin Solid Films **553**, 30–32 (2014). https://doi.org/10.1016/j.tsf.2013.11.069
22. N. Hezil, M. Fellah, J. Aust. Ceram. Soc. **55**, 1167–1175 (2019). https://doi.org/10.1007/s41779-019-00333-7
23. A.A. Pilarska, D. Paukszta, F.C. Sielczyk, T. Jesionowski, Polish. J. Chem. Technol. **12**(2), 52–56 (2010). https://doi.org/10.2478/v10026-010-0018-x
24. Y. Pei, M. Wang, D. Tian, X. Xu, L. Yuan, J. Coll. Interface. Sci. **453**, 194–201 (2015). https://doi.org/10.1016/j.jcis.2015.05.003
25. A. Moradkhani, H.R. Baharvandi, A. Vafaeesefat, M. Tajdari, Int. J. Adv. Design. Manufacturing. Technol. **5**(3), 99–105 (2012)
26. A. Moradkhani, H. Baharvandi, Int. J. Refract. Metal. Hard. Mater. **67**, 40–55 (2017)
27. D. Bouras, A. Mecif, A. Mahdjoub, A. Harabi, M. Zaabat, R. Barille, J. Ovonic Res. **13**, 271–281 (2017)
28. D. Bouras, A. Mecif, R. Barille, A. Harabi, M. Rasheed, A. Mahdjoub, Cu: ZnO. Ceram. Int. **44**(17), 21546–21555 (2018). https://doi.org/10.1016/j.ceramint.2018.08.218
29. E.S. Agorku, A.T. Kuvarega, B.B. Mamba, A.C. Pandey, A.K. Mishra, J. Rare Earths. **33**, 498 (2015). https://doi.org/10.1016/S1002-0721(14)60447-6
30. J. Ma, K. Wang, L. Li, T. Zhang, Y. Kong, S. Komarneni, Ceram. Int. **41**, 2050–2056 (2015). https://doi.org/10.1016/j.ceramint.2014.09.137
31. X. Fu, W. Tang, L. Ji, S. Chen, Chem. Eng. J. **180**, 170–177 (2012). https://doi.org/10.1016/j.cej.2011.11.032

32. M. Fellah, N. Hezil, K. Guerfi, R. Djellabi, A. Montagne, A. Iost, K. Borodin, A. Obrosov, Environ. Sci. Pollut. Res **28**, 7307–7321 (2021). https://doi.org/10.1007/s11356-020-11083-6

33. D. Bouras, A. Mecif, A. Harabi, R. Barillé, A.H. Mahdjoub, M. Zaabat, Catalysts **11**(733), 1–22 (2021). https://doi.org/10.3390/catal11060733

34. D. Xu, L. Li, T. Xia, W. Fan, F. Wang, H. Bai, W. Shi, Int. J. Hydrogen Energy. **43**, 16566–16572 (2018)

35. M. Reli, Int. J. Hydrogen. Energy. **40**, 8530–8538 (2015). https://doi.org/10.1016/J.IJHYDENE.2015.05.004

36. S.G. Patel, J. Chem. Pharmaceut. Res. **7**, 1728–1733 (2015). https://doi.org/10.1515/chem-2017-0002

37. S.R. Meher, Photocatalysis. Micro. Nano. Technologies. (2022). https://doi.org/10.1016/B978-0-12-823018-3.00021-X

38. B. Abebe, H.C.A. Murthy, Mat. Sci. Res. India. (2019). https://doi.org/10.13005/msri/160308

39. S. Kumar, A.K. Ojha, J. Alloys Compd. **644**, 654–662 (2015). https://doi.org/10.1016/J.JALLCOM.2015.04.183

40. P. Bansal, G.R. Chaudhary, S.K. Mehta, Chem. Eng. J. **280**, 475–485 (2015). https://doi.org/10.1016/J.CEJ.2015.06.039

41. W. Dong, J. Wen, Y. Li, C. Wang, S. Sun, D. Shang, Int. J. Pharm. **588**, 119767 (2020)

42. C. Brandes, L. Treccani, S. Kroll, K. Rezwan, J. Am. Ceram. Soc. **97**, 1393–1401 (2014). https://doi.org/10.1111/jace.12877

43. S.N. Basahel, T.T. Ali, M. Mokhtar, K. Narasimharao, Nanoscale Res. Lett. (2015). https://doi.org/10.1186/s11671-015-0780-z

44. D. Bouras, M. Rasheed, R. Barille, M.N. Aldaraji, Opt. Mater. **131**, 112725 (2022). https://doi.org/10.1016/j.optmat.2022.112725